Control of Micro- and Nanocellular Structures in CO_2 Foamed PES/PEN Blends

Luigi Sorrentino,[1,2] Livia Cafiero,[1,3] Salvatore Iannace[1,2]
[1] *Istituto per i Polimeri, Compositi e Biomateriali, Consiglio Nazionale delle Ricerche Piazzale E. Fermi 1, 80055 Portici (NA), Italy*
[2] *IMAST S.c.a.r.l. Distretto Tecnologico sull'Ingegneria dei Materiali Compositi e Polimerici e Strutture Piazza Bovio 22, 80122 Napoli, Italy*
[3] *Università di Napoli, Dipartimenti di Ingegneria Chimica, dei Materiali e della Produzione Industriale Piazzale V. Tecchio 80, 80125 Napoli, Italy*

High performance thermoplastic blends based on polyethersulfone (PES) and poly(ethylene 2,6 naphthalate) (PEN) were foamed with supercritical CO_2 to develop high-performance foams with improved heat deflection temperature, extended processing range, and controlled cellular morphology. The cellular morphology resulted to be strongly influenced by the initial morphology of the blend. The presence of small amount of PES as dispersed phase in PEN based blends acted as blowing agent reservoir and allowed to extend the processing temperature range for obtaining low density foams. The presence of PEN droplets in PES based systems extended the foaming temperatures towards lower values and allowed the development of a bimodal micro/nanocellular morphology at a foaming temperature 60°C lower than the PES glass transition temperature. Furthermore, the presence of PEN droplets compensated for the reduced capability of the host matrix to generate a fine and diffuse porosity at low foaming temperatures. POLYM. ENG. SCI., 55:1281–1289, 2015.

INTRODUCTION

Conventional polymeric foams are employed in many application fields such as packaging, buildings industry, transportation (automotive, aeronautics, naval), or human safety because they are lightweight materials that can combine high specific structural properties (compressive modulus, stress mitigation, cushion, energy absorption) to functional ones (thermal or electric insulation, acoustic insulation or absorption, weight reduction, comfort managing, filtration, thermal stability, fire resistance). Service temperatures in these applications are not much different from the room temperature and foams based on conventional polymers adequately fulfil the performance requirements. In this context, the growing need for weight reduction at high service temperatures is leading to a wider interest in high performance foams.

In this work, poly(ether sulfone) (PES)/poly(ethylene 2,6-naphthalate) (PEN) blends were studied with the aim to develop a thermoplastic matrix with improved heat deflection temperature (HDT), extended processing temperature range, and better control over the foaming process to get a microcellular and/or nanocellular morphology. In particular, the amorphous polymer PES was chosen for its high service temperature ($T_g = 210°C$) while the semicrystalline polymer PEN ($T_g = 125°C$ and $T_m = 265°C$) was selected due to its ability to obtain low density foams (lower than 0.15 g/cm^3) by means of supercritical CO_2. Closed cell PEN foams were, for the first time, investigated by our research group using the batch foaming technique [1–3]. Microcellular structures with controlled density (from 0.12 to 0.60 g/cm^3) and cell size (from 5 and 15 μm) were obtained by using supercritical carbon dioxide in a wide range of temperatures (from 100°C to 240°C). Foams from PES were prepared in 2001 by Krause et al. [4], by using carbon dioxide as physical blowing agent. They obtained foams characterized by a microcellular closed cell morphology with density higher than 0.4 g/cm^3.

Polymer blending has been used in foaming to increase the strain hardening and other rheological properties of the host polymer [5, 6], to utilize interfaces in immiscible blends for heterogeneous cell nucleation [7, 8], to adjust the open/closed cell content [9–11], to control the absorption of the foaming agent [12–15] and to tailor the mechanical strength [16, 17]. Moreover, the nonhomogeneous phase morphology of immiscible polymeric blends and the differences in the elasticity as well as in the gas solubility between the polymers can be exploited to promote the formation of microcellular or nanocellular structure. Typical polymer blends used for microcellular foaming mainly include polypropylene (PP)/polyethylene (PE) [18–21] and polystyrene (PS)/poly(methyl methacrylate) (PMMA) [22–24], while nanocellular foams have been developed from PP/thermoplastic elastomer blends [25, 26].

Few works report on the foaming of blends of high performance polymers. Foams based on poly(ether imide) (PEI)/PES fully amorphous blends were characterized by the presence of cellular structures in both polymeric phases [4]. In poly(ether ether ketone) (PEEK)/PEI semicrystalline/amorphous blends cells were only present in the PES phase due to the selective solubilization of CO_2 into the amorphous phase and to the poor foaming behavior of PEEK in the used experimental conditions [27].

In this context, PES/PEN amorphous/semicrystalline blends were investigated with the aim of developing high performance foams with micro-/nanocellular morphology. In this regard, the role of composition, processing conditions and blend morphology on the cellular structure of the foamed blend were investigated.

Correspondence to: Luigi Sorrentino; e-mail: luigi.sorrentino@cnr.it
Contract grant sponsor: MIUR Ministry (Italy) (TECOP project); contract grant number: PON02_00029_3206010).
DOI 10.1002/pen.24066
Published online in Wiley Online Library (wileyonlinelibrary.com).

EXPERIMENTAL

Raw Materials and Blends Preparation

PES and PEN in pellet form were purchased from BASF (density of 1.37 g/cm^3, Ultrason E3010, BASF, Germany) and Teijin Kasei (density of 1.36 g/cm^3, Teonex TN8065S, Teijin, Japan), respectively. The physical blowing agent was carbon dioxide (purity = 99.9%, Società Ossigeno Napoli, Italy). Pellets of PES/PEN blends with different compositions (90/10, 75/25, 25/75, 10/90 percent by weight) were prepared by using a twin screw extruder (Rheocord PTW25P, Haake, Germany). The extrusion temperatures were adjusted between 290 and 300°C depending on the blend composition, while the screw speed was kept constant and equal to 70 rpm in order to assure a residence time of 5 min.

Samples Preparation

A hydraulic press (model P300P, from Collin GmbH, Germany) was used to prepare 1 mm thick slabs through compression molding at 290°C. To avoid the crystallization of PEN during cooling, the slabs were quenched from the melt state by immersing them in cold water (kept at 10°C) for 120 s. Specimens were then cut from the quenched slabs and vacuum dried at 120°C for 24 h. The blowing agent sorption was performed in a high pressure vessel operated at 8.0 MPa and 50°C for 72 h. After the evaluation of the gas uptake, the samples were then foamed as described below.

Thermal and Thermomechanical Properties of Blends

Crystallization and melting properties of the PEN phase were analyzed by differential scanning calorimetry with a DSC 2920 (TA Instruments, New Castle, DE) since they can affect its foaming properties. In particular, DSC scans from the melt state were performed on neat PEN samples at different cooling rates (1, 2, 5, 10°C/min). Subsequent heating scans were performed at heating rate equal to 10°C/min. The degree of crystallinity of the PEN phase was calculated by taking into account the melting enthalpy of the perfect crystal (ΔH_m° = 190 J/g from Ref. [28]).

Dynamic mechanical (DMA) properties were evaluated with a dynamic mechanical analyzer (Triton 2000, Tritontech, UK) by using the single cantilever geometry on samples (30 mm × 10 mm in size) cut from molded slabs. The oscillation amplitude and the frequency of DMA tests were set to 50 μm and 1 Hz, respectively.

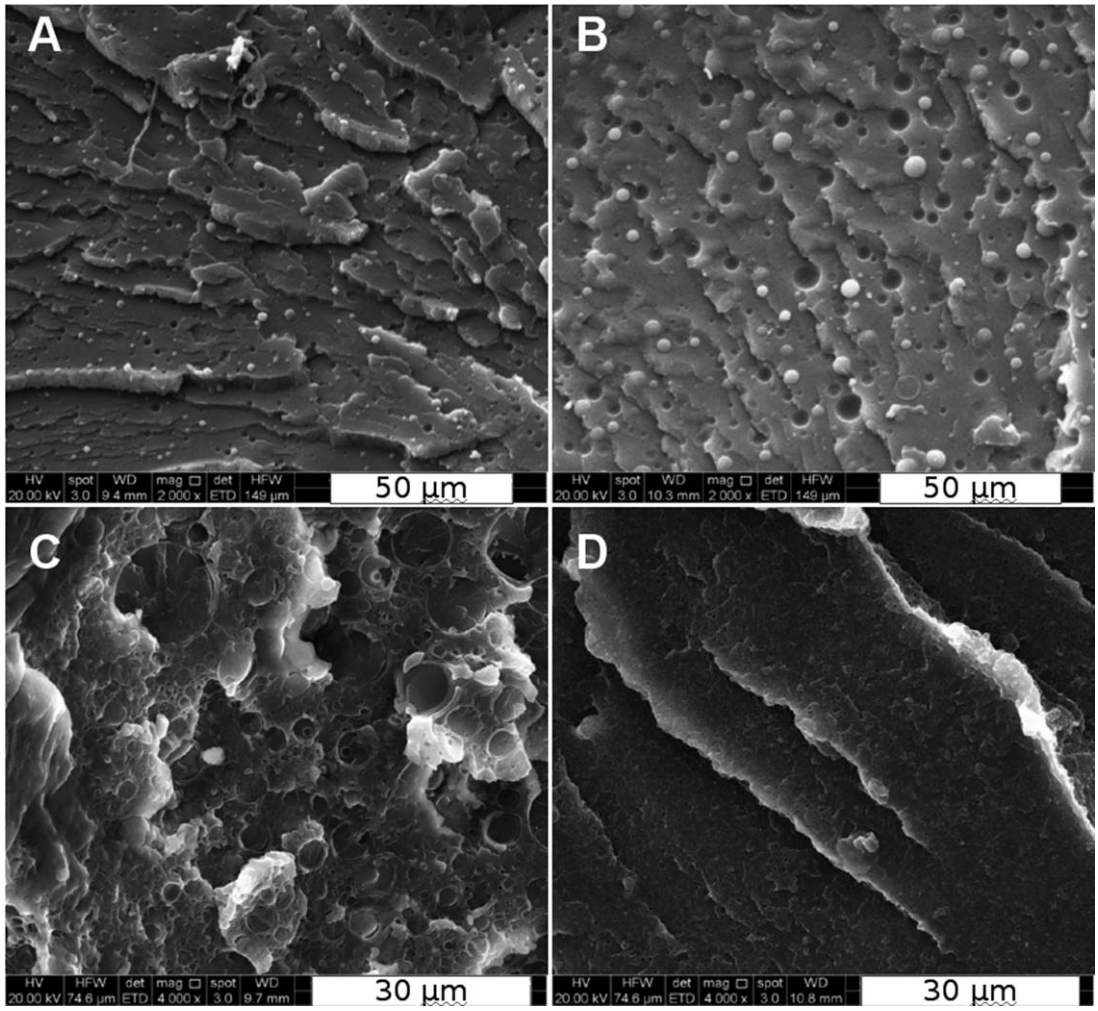

FIG. 1. SEM micrographs of fractured surfaces of samples cut from molded slabs showing the blend morphology: (A) PES/PEN 10/90; (B) PES/PEN 25/75; (C) PES/PEN 75/25; (D) PES/PEN 90/10.

 DOI 10.1002/pen

Foaming Process and Foams Analysis

Foams were prepared by using the solid state foaming technique. Rectangular samples (30 mm × 10 mm in size) were foamed, after gas sorption, by immersion in a bath containing silicon oil at the desired foaming temperature (160, 180, 200, and 220°C). After foaming, always occurring within 10 s, foamed samples were quenched in cold water to stabilize the cellular structure. The foam density was measured by using the water displacement method according to ASTM D792. Scanning electron microscopy (SEM) analysis was performed on cryogenic fractured surfaces by using a Quanta 200 FEG (FEI, The Nederlands).

RESULTS AND DISCUSSION

Blends Morphology

SEM micrographs of fractured surfaces from blends samples are reported in Fig. 1. The heterogeneous morphology present in all samples is a direct evidence of the immiscibility of PES and PEN in the investigated compositions. Spherical droplets of PES were observed in the PES/PEN 10/90 (average size of 1.5 μm, Fig. 1A) and 25/75 (average size of 3.5 μm, Fig. 1B) blends while spherical droplets of PEN were formed in the PES/PEN 75/25 (average size of 1.5 μm, Fig. 1C) and 90/10 (average size of 0.7 μm, Fig. 1D) blends. The measured mean droplet size was in proportion to the polymer viscosity (mean PES droplet size was found larger than mean PEN droplet size for the same dispersed phase content due to the lower viscosity of PEN with respect to PES at the same temperature) and to the amount of dispersed phase (the largest mean droplet size occurred in blends with 25 wt% dispersed phase). Furthermore, the very small size of PEN droplets in the PES/PEN 90/10 blend is likely to be responsible for the lower degree of crystallinity, as discussed below.

Thermal Behavior

As reported in Table 1, the enthalpy of crystallization of neat PEN decreased with the increase of cooling rate. In particular, at a cooling rate equal to 5°C/min, the crystallization peak was barely visible (Fig. 2), while at 10°C/min no crystallization peak was clearly detectable. Cold crystallization phenomena occurred during the subsequent heating scans performed at 10°C/min. However, as reported in Table 1, the amount of crystallinity developed during the heating scan was fairly low compared to the amount of crystallinity developed during the cooling scan. These results showed that to obtain amorphous PEN samples a cooling rate of at least 10°C/min should be used. Unlike in neat PEN, exothermic peaks were

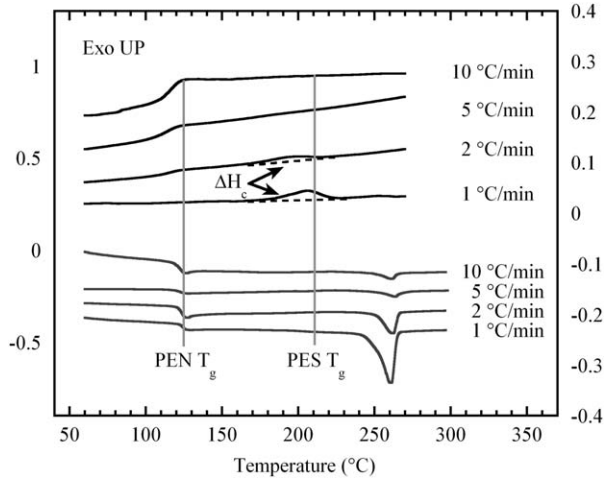

FIG. 2. Effects of cooling rates on the crystallization behavior of Neat PEN: upper group of lines refer to cooling scans from the melt state at the specified cooling rate; lower group of lines refer to heating scans, all performed at 10°C/min, of samples cooled at the specified cooling rate

detected in DSC plots of the blends during the cooling scan at 10°C/min, as shown in Fig. 3A. A crystalline phase was thus developed in blends during their cooling. The degree of crystallinity (X_c), calculated as the mass fraction of crystals in the PEN phase, was found to be dependent on the PES/PEN composition. As reported in Table 2, X_c was higher in blends containing 90% and 75% of PEN with respect those containing a low PEN amount (25% and 10%). During the heating scan on quenched samples the heat flow released due to the formation of crystals was, in all blends, almost equal to the heat flow absorbed to melt PEN crystals. This confirmed that crystals did not form during the quenching from the melt state in any blend and that quenched samples can be considered as blends of amorphous polymers.

The heating scans performed on quenched samples (Fig. 3B) show the occurrence of a remarkable cold crystallization of PEN. This suggests that the PES phase promotes the nucleation of crystals in PEN both from the melt state and in the solid state, and that the nucleating effect is more remarkable when PES is the dispersed phase.

In order to maximize the mechanical response and to verify if an increase of the service temperature could be obtained, samples of each blend were thermally conditioned to allow the full crystallization of the PEN phase. In particular, amorphous blend samples were kept for 30 min at 200°C, which was the onset temperature of the cold crystallization as evaluated from DSC heating scans (Fig. 3B). The results of DSC scans performed on

TABLE 1. Enthalpy of crystallization (ΔH_c), enthalpy of melting (ΔH_m), and melting temperature (T_m) of neat PEN samples at different cooling rates.

Cooling scan			Heating scan			
Cooling rate (°C/min)	ΔH_c (J/g)	Peak T_c (°C)	Heating rate (°C/min)	ΔH_c (J/g)	ΔH_m (J/g)	Peak T_m (°C)
1	18.70	205.8	10	2.80	21.50	260.6
2	6.20	195.3	10	0.47	6.74	262.3
5	4.19	225.3	10	1.20	5.40	263.6
10	0.00	–	10	1.33	1.33	261.4

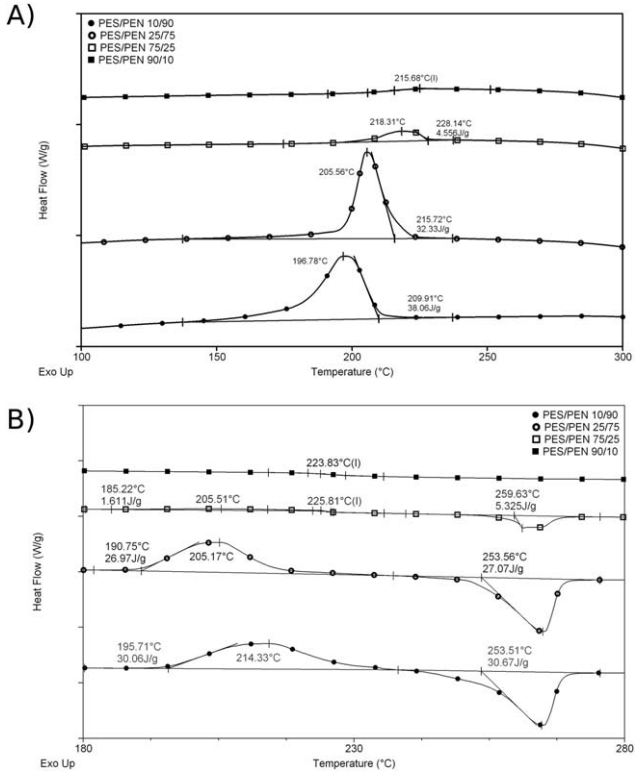

FIG. 3. DSC scans of PES/PEN blends (*y*-axis division is equal to 0.5 W/g). (A) cooling scans from the melt state (10°C/min), (B) heating scan on quenched samples (10°C/min).

crystallized samples are reported in Table 2. The melting temperature of the PEN phase in crystallized blends was independent on the blend composition, suggesting that the crystalline structure was not affected by the presence of PES. However, remarkable differences were observed in the degree of crystallinity as a function of the blend composition. The X_c calculated for blends containing 10% ($X_c = 2.9\%$) and 25% of PEN ($X_c = 10.7\%$) was lower than the X_c calculated for neat PEN ($X_c = 18.2\%$) and the PEN rich blends ($X_c = 21.2\%$ for PES/PEN 25/75 and $X_c = 20.3\%$ for PES/PEN 10/90). These results suggest that the crystallization of PEN macromolecules was hindered within the dispersed droplets, as a consequence of their size. As shown above, the average size of PEN droplets is significantly lower than 1 μm, therefore the growth of well-developed crystals can be limited by the small droplet volume.

TABLE 2. Degree of crystallinity (X_c), crystallization temperature (T_c), melting temperature (T_m), enthalpy of crystallization (ΔH_c), and of melting (ΔH_m) of PEN measured during cooling from the melt state and during heating from room temperature.

	Cooling scan from the melt			Heating scan after crystallization		
Sample	X_c (%)	T_c (°C)	ΔH_c (J/g)	X_c (%)	T_m (°C)	ΔH_m (J/g)
Neat PEN	/	/	/	18.2	265.7	34.62
Neat PES	/	/	/	/	/	/
PES/PEN 90/10	12.2	225.7	2.32	2.9	264.8	0.55
PES/PEN 75/25	10.5	218.7	4.97	10.7	265.4	5.06
PES/PEN 25/75	19.9	205.6	28.29	21.2	266.2	30.23
PES/PEN 10/90	21.7	198.1	37.02	20.3	265.6	34.71

X_c values were normalized by the actual PEN content in the blend.

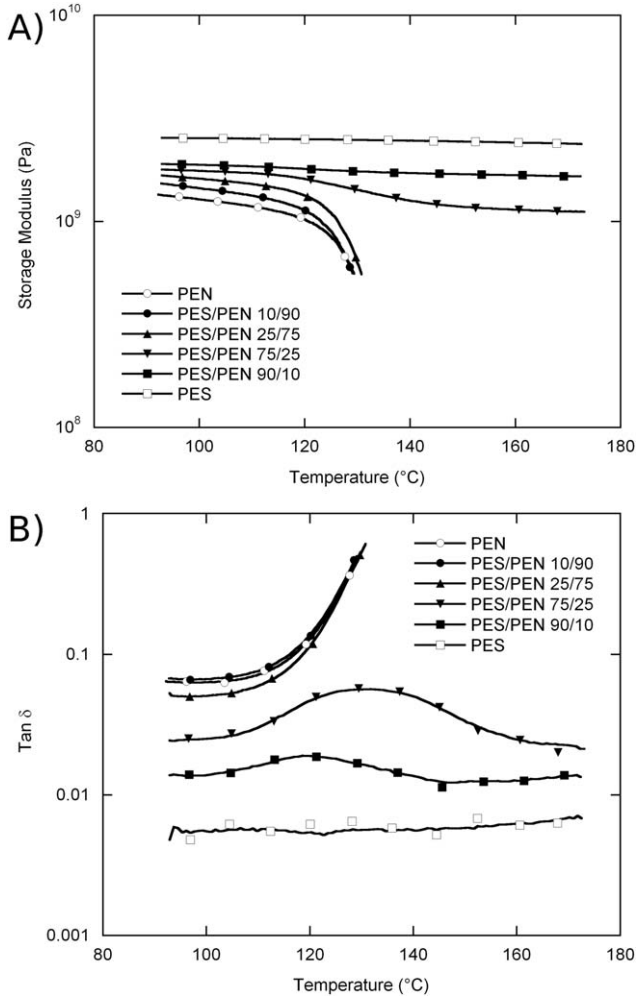

FIG. 4. Dynamic–mechanical properties of quenched PES/PEN blends: (A) Storage modulus, (B) Tan δ.

Dynamic Mechanical Behavior

In order to investigate the effects of blending on the service temperatures of PES/PEN blends for potential use in high performance applications, the storage modulus and the tan δ of both amorphous and isothermally crystallized samples were evaluated (Figs. 4 and 5). The presence of PES droplets in PEN rich amorphous blends (quenched samples) moderately increased the storage modulus above the glass transition of PEN (Fig. 4). Conversely, PES droplets in crystallized samples showed an enhanced onset of storage modulus drop, far above the glass transition temperature of the neat matrix (Fig. 5) and resulted in a significant improvement of the service temperature in comparison to neat PEN. In PES rich blends, the dynamic mechanical response was mainly influenced by the properties of the host phase. For these blends, the storage modulus did not drop above the T_g of the PEN phase and remained significantly high up to the T_g of PES. It is worth noting that the T_g of the PEN phase, measured at the peak of tan δ, was lower in blends containing lower amount of PEN (10 and 25%). According to DSC results, this behavior can be associated with the lower degree of

 DOI 10.1002/pen

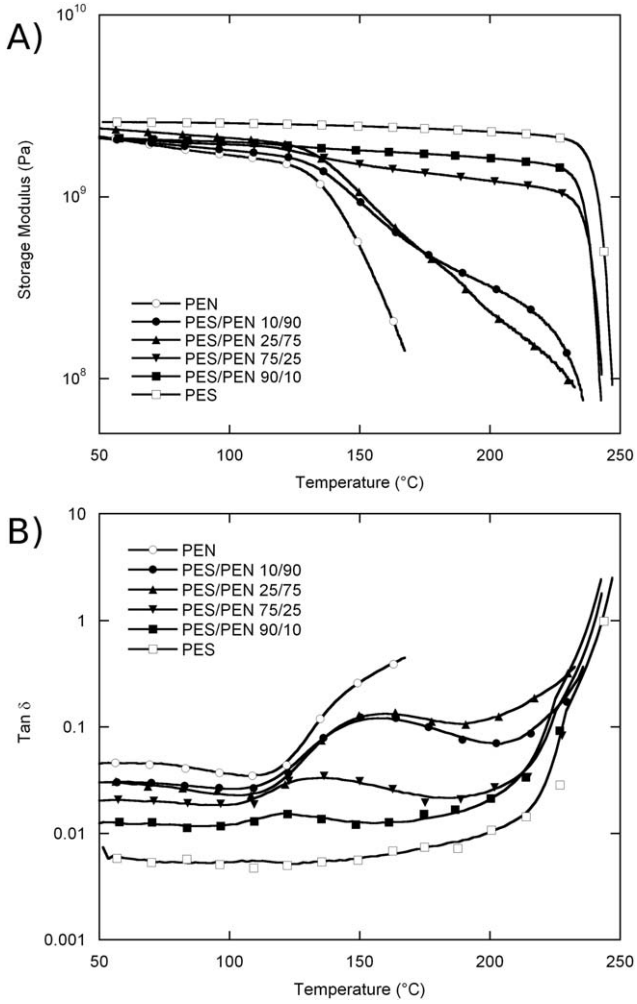

FIG. 5. Dynamic−mechanical properties of PES/PEN blends after crystallization of PEN phase at 200°C for 30 min: (A) Storage Modulus, (B) Tan δ.

crystallinity developed in PEN when dispersed as small droplets in PES.

Foaming Behavior

Figure 6 shows the effect of the foaming temperature on the density of foamed blends. The CO_2 uptake of blends after 72 h at 50°C and 8.0 MPa is reported in the same figure. The amount of CO_2 absorbed is higher in the PES phase. In particular, after the soaking time the CO_2 concentration was 8% in neat PES and 4.7% in neat PEN. Because of the larger amount of gas solubilized in the PES phase, the total amount of CO_2 absorbed by the blends increased monotonically with the increase of PES amount. However, due to the different diffusivity of the gas in the two parent polymers and since the polymer/gas systems are not yet at the equilibrium, the overall CO_2 uptake in the blend cannot be calculated as the weighted average of the gas absorbed by the pure polymers.

The effect of the blend composition on the final density of foams was dependent on both foaming properties of the host phase (in general PEN rich blends showed lower densities than PES rich ones) and the foaming temperature. The density of PES based systems was significantly lowered by increasing the foaming temperature from 160 to 200°C. Minor reductions were

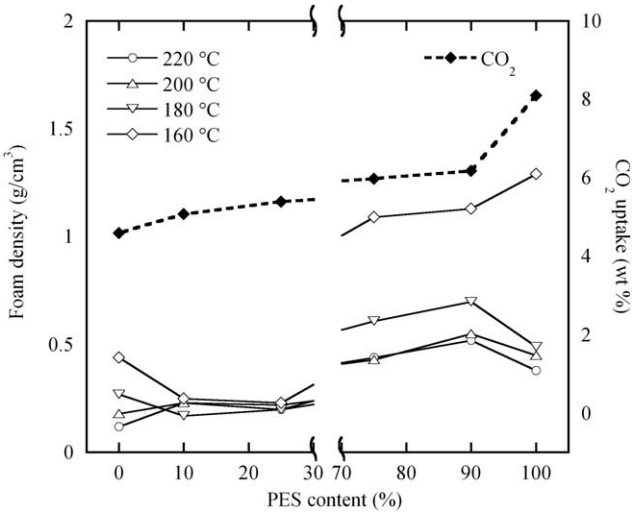

FIG. 6. CO_2 uptake in PES/PEN blends after gas sorption and density of samples foamed at different temperatures as a function of PES content.

observed when the foaming temperature was increased from 200 to 220°C. The density of PEN rich blends was also reduced by an increase of the foaming temperature, even if at a minor extent.

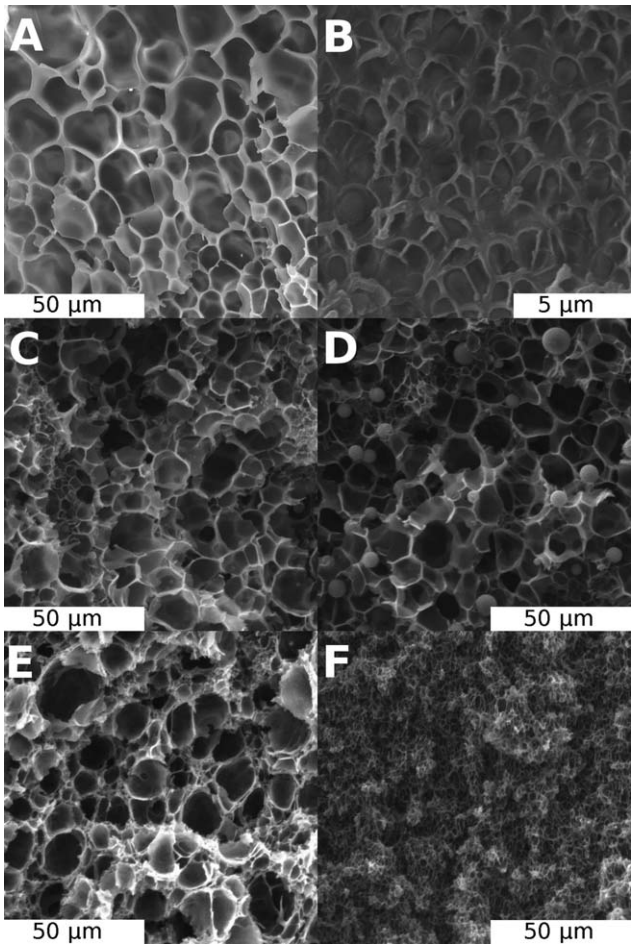

FIG. 7. SEM micrographs of foamed blends showing the morphologies obtained after foaming at 180°C: (A) Neat PEN, (B) Neat PES, (C) PES/PEN 10/90, (D) PES/PEN 25/75, (E) PES/PEN 75/25, (F) PES/PEN 90/10.

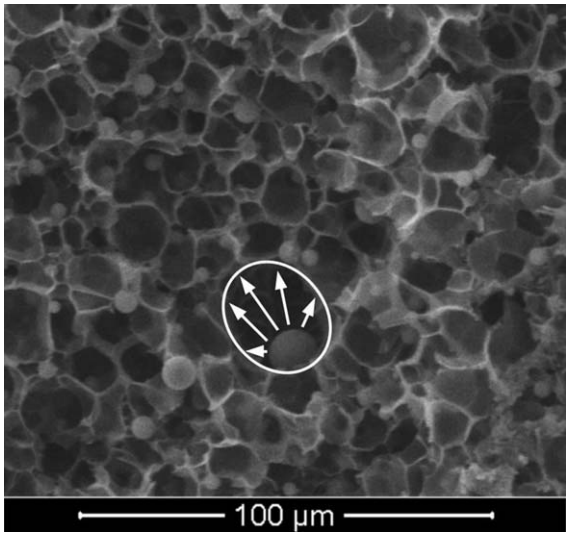

FIG. 8. Expanded PES droplets as reservoir of CO_2 for further PEN expanding in PES/PEN 25/75 blend.

Figure 7 shows the cellular morphologies of neat PEN, neat PES and their blends foamed at 180°C. At this temperature the cellular structure of neat PEN foams was characterized by cells having a mean diameter greater than 10 μm while very small cells, having a mean diameter of less than 2 μm, were observed in neat PES foams. It is worth noting that PES was foamed at temperatures much lower than its T_g due to the strong plasticization effect of the solubilized CO_2 [4]. At 180°C the density of neat PES samples was 0.49 g/cm^3, while that of neat PEN foams was 0.27 g/cm^3 in the applied foaming conditions. The cellular morphology of foamed blends was strongly dependent on the blend composition and the starting morphology. A bimodal cellular morphology was evident in most of the blends except for PES/PEN 90/10, which exhibited a monomodal distribution of small cells. The presence of cells with two distinct mean sizes (10 μm and 2 μm) suggests that PEN and PES expanded to a different extent also in their blends. The density of foamed blends containing PES droplets (PES/PEN 10/90 and 25/75) was around 0.2 g/cm^3, showing that the overall expansion ratio was mainly controlled by the foaming properties of PEN. Much higher densities were obtained in blends having higher content of PES: 0.7 g/cm^3 in PES/PEN 90/10 and 0.6 g/cm^3 in PES/PEN 75/25 (both values from the foaming test at 180°C). The PES phase determined the final density of these foams and constrained the small PEN droplets to a lower expansion ratio.

A very interesting finding is that at both 160°C and 180°C the foam density of PEN rich blends resulted lower than that of neat PEN. In particular, in the PES/PEN 25/75 blend large voids around expanded PES droplets were often observed (Fig. 8), suggesting that the PES phase may work as CO_2 reservoir to support both the nucleation at the PES/PEN interface and the further growth of nucleated bubbles through the gas escaping into PEN from consolidated, not further expanding PES droplets. As mentioned above, the PES phase absorbs more CO_2 at the same saturation temperature and pressure than the PEN one. When the temperature is increased, the system shift away from the equilibrium state and the CO_2 concentration gradient across the PES/PEN interface causes the diffusion of CO_2 from PES droplets into PEN ones, at a rate depending on the actual CO_2 concentration and solubility in each phase. Thus, the extra CO_2 coming into the PEN phase might both prolong its supersaturated condition, leading to additional cell nucleation, and further inflate previously nucleated bubbles.

TABLE 3. Data of PES/PEN 25/75 samples foamed at 180°C as a function of the annealing time.

Crystallization time (min)	X_c (%)	Density (g/cm^3)	Expansion ratio of PES drops
0	1.2	0.21	2.3
2.5	3.2	0.23	2.2
5.0	6.2	0.23	2.3
10	11.5	0.28	2.9
12.5	15.8	0.37	2.9

To investigate how the presence of PEN crystals could affect the cellular morphology, certain degrees of crystallinity (reported in Table 3) were induced in several samples of the PES/PEN 25/75 blend by means of an annealing procedure. In particular, blend samples were isothermally crystallized at 180°C for different time intervals (annealing time of 2.5, 5, 10, and 12.5 min) and then solubilized with the blowing agent. Figure 9 shows the effect of the annealing time by plotting the density of the foamed blend and the mean size of expanded PES droplets as a function of the induced degree of crystallinity. The cellular morphology of these samples is shown in Fig. 10. The foam density is not significantly influenced up to an annealing time of 5 min; hence, a relative crystallinity of 6.2% does not significantly affect neither the capability of PEN to reach a low density nor the size of expanded PES droplets. After an annealing time of 10 min, the degree of crystallinity of PEN increased above 11% and the density of the foamed blend significantly raised. It is worth noting that in this condition the mean size of expanded PES droplets also increased, confirming that viscoelastic and gas transport properties of the host matrix could affect the nucleation and growth behavior of the dispersed phase. The increased size of expanded PES droplets in samples with high X_c is an indirect confirmation of the mechanism assumed above. In particular, the increase of X_c in PEN

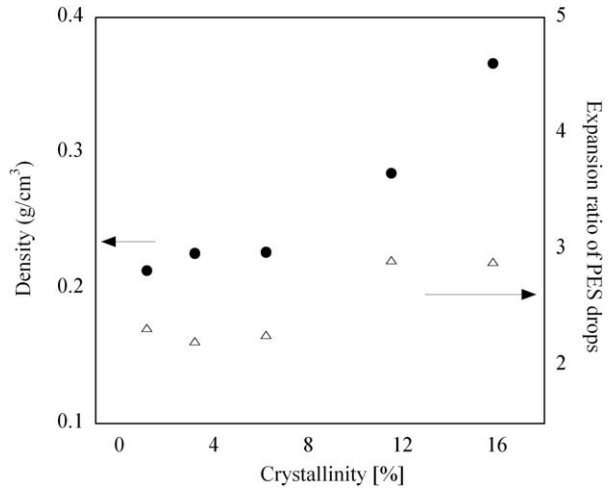

FIG. 9. Average size of expanded PES droplets and density of the PES/PEN 25/75 foam after the isothermal crystallization at 180°C.

DOI 10.1002/pen

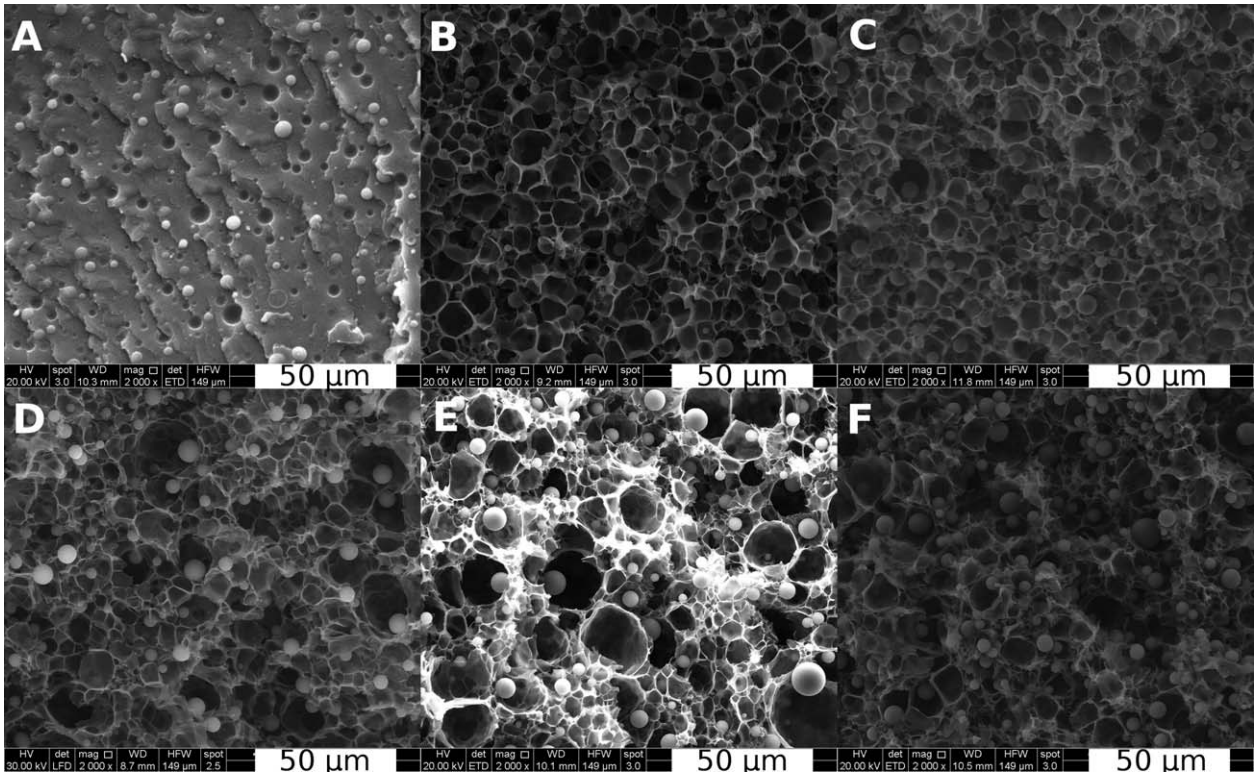

FIG. 10. SEM micrographs of the blend PES/PEN 25/75 showing the effect of the annealing time on the cellular morphology: (A) unfoamed blend, (B) not crystallized blend, (C) 2.5 min, (D) 5 min, (E) 10 min, (F) 12.5 min.

increases its viscosity and reduces its gas transport properties (solubility and diffusivity), in turn acting as an improved "barrier" to the diffusion of CO_2 from the dispersed phase (PES droplets) to the host matrix (PEN). Therefore, the concentration of CO_2 in the PES phase is kept high for longer time, allowing for a further growth of dispersed droplets.

Micro-/nanocellular foams were obtained from PES rich blends at the lowest investigated foaming temperature. As shown in Fig. 11(A), the temperature of 160°C is low enough to hinder or strongly limit the formation of a well-developed cellular structure in neat PES, due to the high viscosity of the plasticized host phase and the small number of nucleated cells. Only a marginal reduction of the apparent density was achieved (the foam density was equal to 1.29 g/cm^3). The presence of 10% of PEN in the blend allowed for the formation of a micro-/nanocellular structure (Fig. 11B) characterized by bubbles having size within the 0.3−1.5 μm range and foam density of about 1.13 g/cm^3, while a higher content of PEN (25 wt%) led to a micro-/nanocellular cellular structure (Fig. 11C) with cell size within the 0.6−5 μm range and further lower density (1.09 g/cm^3). As mentioned in the Introduction paragraph, the formation of microcellular and nanocellular foams in blends has been recently investigated. For example, Otsuka et al. [22] developed nanocellular foams having an average pore diameter of 40−50 nm and a pore density of 8.5×10^{14} cm^{-1} from PS/PMMA blends. They utilized the blend morphology, the different CO_2 solubility and the viscoelasticity of the two polymers to control the bubble nucleation sites and the bubble growth.

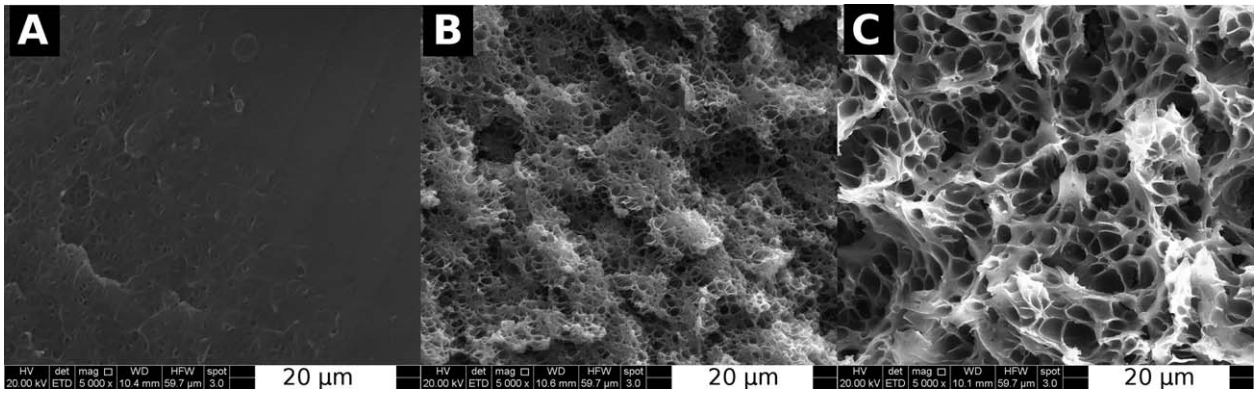

FIG. 11. SEM micrographs of samples foamed at 160°C: (A) Neat PES, (B) PES/PEN 90/10, and (C) PES/PEN 75/25.

Similarly to the present work, they set foaming temperatures lower than the T_g of the polymers ensuring the suppression of bubble growth by the stiffness increase in the host polymer. Unlike in their PS/PMMA system, where the CO_2 solubility was higher in the dispersed droplets (similarly to PEN rich blends investigated in the present work), in PES rich systems the solubility was higher in the host matrix. With our approach the direct foaming of the PES phase, although kept in a plasticized condition with lower viscoelasticity, was strongly limited or hindered. At the same time, in these conditions the interface between PEN droplets and the surrounding matrix could act as a thermodynamic confinement to the CO_2 escape from the scarcely solubilized phase (PEN) to the highly solubilized one (PES). The overall result was that PEN bubbles were not only able to nucleate and grow but they were also further inflated by the CO_2 coming from the highly solubilized host phase, which again acted as a blowing agent reservoir.

CONCLUSIONS

The role of composition, morphology, and processing conditions on the crystallization, melting, and dynamic mechanical behavior of PES/PEN blends was analyzed with the aim of controlling the size and location of bubbles generated during their foaming. The investigated polymers resulted to be immiscible and showed a morphology characterized by spherical droplets dispersed in a continuous matrix. The degree of crystallinity developed in the PEN phase was dependent on the blend composition. In particular, the presence of PES as dispersed phase promoted the nucleation of crystals in the PEN phase. The nucleating effect was particularly evident when PES droplets had a very small size. The DMA characterization performed on PEN rich samples after being annealed showed that the presence of a small amount of PES enhanced the heat deflection temperature far above the glass transition temperature of neat PEN.

High performance micro-/nanocellular foams were successfully prepared by using carbon dioxide as blowing agent. The minimum density of foams from PEN rich blends, prepared at 180°C, was 0.2 g/cm^3, a value lower than the density of foams obtained from neat PEN at the same foaming temperature. This finding was related to the higher solubility of CO_2 in PES than in PEN. The highly saturated PES droplets worked as CO_2 reservoir for further nucleation and growth of PEN bubbles as a consequence of the CO_2 diffusion from the highly saturated phase to the lowly saturated one. In PES rich blends, a bimodal cellular size distribution developed as a result of the different elasticity of the two polymers.

Moreover, foams were successfully obtained in PEN rich blends after a crystallization treatment. Above a X_c value of 6.2%, the expansion ratio of the PEN phase was in inverse relation to X_c. In the same conditions the expansion ratio of the dispersed PES droplets clearly increased. This result demonstrates that the formation of a crystalline phase in PEN (host matrix) reduced the gas escape through the PES/PEN interface, allowing a further expansion of the dispersed droplets.

By lowering the foaming temperature to 160°C, the addition of a small amount of PEN in PES led to the formation of micro-/nanocellular foams with cell size of 0.3−1.5 μm in the PES/PEN 90/10 blend and of 0.6−5 μm in PES/PEN 75/25 blend. The interface between the host PES (containing higher concentration of gas) and PEN can act as a thermodynamic confinement to the CO_2 escape from PEN droplets to the outside. Conversely, in these conditions the expansion only occurred in the dispersed phase (PEN), whose expansion was enhanced by the blowing agent drained from the highly solubilized PES.

ACKNOWLEDGMENTS

The authors would like to thank Mr Fabio Docimo for its contribution to the preparation of all tested samples.

REFERENCES

1. L. Sorrentino, M. Aurilia, and S. Iannace, *Adv. Polym. Tech.*, **30**, 234 (2011).
2. L. Sorrentino, M. Aurilia, L. Cafiero, and Iannace, S. *J. Appl. Polym. Sci.*, **122**, 3701 (2011).
3. L. Sorrentino, M. Aurilia, L. Cafiero, S. Cioffi, and S. Iannace, *J. Cell. Plast.*, **48**, 355 (2012).
4. B. Krause, H.J.P. Sijbesma, P. Münüklü, N.F.A. van der Vegt, and M. Wessling, *Macromolecules*, **34**, 8792 (2001).
5. R. Dhavalikar, M. Yamaguchi, and M. Xanthos, *J. Polym. Sci. Part A Polym. Chem.* **41**, 958 (2003).
6. N. Reichelt, M. Stadlbauer, R. Folland, C.B. Park, and J. Wang, *Cell. Polym.*, **22**, 315 (2003).
7. N.S. Ramesh, D.H. Rasmussen, and G.A. Campbell, *Polym. Eng. Sci.* **34**, 1685 (1994).
8. N.S. Ramesh, D.H. Rasmussen, and G.A. Campbell, *Polym. Eng. Sci.*, **34**, 1698 (1994).
9. B. Krause, K. Diekmann, N.F.A. van der Vegt, and M. Wessling, *Macromolecules*, **35**, 1738 (2002).
10. B. Krause, G.-H. Koops, N.F.A. van der Vegt, M. Wessling, M. Wübbenhorst, and J. van Turnhout, *Adv. Mater.*, **14**, 1041 (2002).
11. B.I. Chaudhary, R.P. Barry, and M.H. Tusim, *J. Cell. Plast.*, **36**, 397 (2000).
12. R.H.B. Bouma, W.J. Nauta, J.E.F. Arnauts, T. van Den Boomgaard, J.M. Steuten, and H. Strathmann, *J. Appl. Polym. Sci.*, **65**, 2679 (1997).
13. J. Wang, C. Xingguo, Y. Mingjun, and H. Jiasong, *Polymer*, **42**, 8265 (2001).
14. S. Siripurapu, Y.J. Gay, J.R. Royer, J.M. DeSimone, R.J. Spontak, and S.A. Khan, *Polymer*, **43**, 5511 (2002).
15. T.A. Walker, S. Siripurapu, J.L. Young, S.G. Hirsch, S.A. Khan, J.M. DeSimone, and R.J. Spontak, *Abstr. Pap. Am. Chem. Soc.*, **221**, U375 (2001).
16. I.-C. Liu, C.-K. Chuang, and R.C-C. Tsiang, *J. Polym. Res.*, **11**, 149 (2004).
17. M.A. Rodriguez-Perez, A. Duijsens, and J.A. De Saja, *J. Appl. Polym. Sci.*, **68**, 1237 (1998).
18. P. Rachtanapun, S.E.M. Selke, and L.M. Matuana, *Polym. Eng. Sci.*, **44**, 1551 (2004).
19. H.-X. Huang and J.-K. Wang, *J. Appl. Polym. Sci.*, **106**, 505 (2007).
20. H.-X. Huang, J.-K. Wang, and X.-H. Sun, *J. Cell. Plast.*, **44**, 69 (2008).
21. S. Doroudiani, C.B. Park, and M.T. Kortschot, *Polym. Eng. Sci.*, **38**, 1205 (1998).
22. T. Otsuka, K. Taki, and M. Ohshima, *Macromol. Mater. Eng.*, **293**, 78 (2008).

 DOI 10.1002/pen

23. X. Han, J. Shen, H. Huang, D.L. Tomasko, and L.J. Lee, *Polym. Eng. Sci.*, **47**, 103 (2007).
24. D. Kohlhoff, A. Nabil, and M. Ohshima, *Polym. Adv. Technol.*, **23**, 1350 (2012).
25. T. Nemoto, J. Takagi, and M. Ohshima, *Macromol. Mater. Eng.*, **293**, 991 (2008).
26. T. Nemoto, J. Takagi, and M. Ohshima, *Macromol. Mater. Eng.*, **293**, 574 (2008).
27. T. Nemoto, J. Takagi, and M. Ohshima, *Polym. Eng. Sci.*, **50**, 2408 (2010).
28. S.H. Kim, S.M. Hong, S.S. Hwang, and H.O. Yoo, *J. Appl. Polym. Sci.*, **74**, 2448 (1999).